doi:10.1093/brain/awt113 Brain 2013: 136; 1718–1731 | 1718

BRAIN
A JOURNAL OF NEUROLOGY

Deleting exon 55 from the nebulin gene induces severe muscle weakness in a mouse model for nemaline myopathy

Coen A. C. Ottenheijm,[1,2] Danielle Buck,[2] Josine M. de Winter,[1] Claudia Ferrara,[3] Nicoletta Piroddi,[3] Chiara Tesi,[3] Jeffrey R. Jasper,[4] Fady I. Malik,[4] Hui Meng,[5] Ger J. M. Stienen,[1,6] Alan H. Beggs,[7] Siegfried Labeit,[8] Corrado Poggesi,[3] Michael W. Lawlor[5] and Henk Granzier[2]

1 Department of Physiology, VU University Medical Centre, Amsterdam, The Netherlands
2 Department of Physiology, University of Arizona, Tucson, AZ, USA
3 Department of Physiology, University of Florence, Florence, Italy
4 Research and Early Development, Cytokinetics, Inc., South San Francisco, CA, USA
5 Division of Paediatric Pathology, Department of Pathology and Laboratory Medicine, Medical College of Wisconsin, Milwaukee, WI, USA
6 Department of Physics and Astronomy, VU University, Amsterdam, The Netherlands
7 Division of Genetics and Program in Genomics, The Manton Centre for Orphan Disease Research, Boston Children's Hospital, Harvard Medical School, Boston, MA, USA
8 Department for Integrative Pathophysiology, Medical Faculty Mannheim, University of Heidelberg, Germany

Correspondence to: Henk Granzier,
Department of Physiology,
University of Arizona, P.O. Box 245217,
Tucson, AZ 85724, USA
E-mail: granzier@email.arizona.edu

Nebulin—a giant sarcomeric protein—plays a pivotal role in skeletal muscle contractility by specifying thin filament length and function. Although mutations in the gene encoding nebulin (*NEB*) are a frequent cause of nemaline myopathy, the most common non-dystrophic congenital myopathy, the mechanisms by which mutations in *NEB* cause muscle weakness remain largely unknown. To better understand these mechanisms, we have generated a mouse model in which *Neb* exon 55 is deleted ($Neb^{\Delta Exon55}$) to replicate a founder mutation seen frequently in patients with nemaline myopathy with Ashkenazi Jewish heritage. $Neb^{\Delta Exon55}$ mice are born close to Mendelian ratios, but show growth retardation after birth. Electron microscopy studies show nemaline bodies—a hallmark feature of nemaline myopathy—in muscle fibres from $Neb^{\Delta Exon55}$ mice. Western blotting studies with nebulin-specific antibodies reveal reduced nebulin levels in muscle from $Neb^{\Delta Exon55}$ mice, and immunofluorescence confocal microscopy studies with tropomodulin antibodies and phalloidin reveal that thin filament length is significantly reduced. In line with reduced thin filament length, the maximal force generating capacity of permeabilized muscle fibres and single myofibrils is reduced in $Neb^{\Delta Exon55}$ mice with a more pronounced reduction at longer sarcomere lengths. Finally, in $Neb^{\Delta Exon55}$ mice the regulation of contraction is impaired, as evidenced by marked changes in crossbridge cycling kinetics and by a reduction of the calcium sensitivity of force generation. A novel drug that facilitates calcium binding to the thin filament significantly augmented the calcium sensitivity of submaximal force to levels that exceed those observed in untreated control muscle. In conclusion, we have characterized the first nebulin-based nemaline myopathy model, which recapitulates important features of the phenotype observed in patients harbouring this particular mutation, and which has severe muscle weakness caused by thin filament dysfunction.

Keywords: nebulin; nemaline myopathy; muscle fibre weakness; thin filament function

Received December 20, 2012. Revised March 15, 2013. Accepted March 18, 2013

Introduction

Nemaline myopathy is the most common non-dystrophic congenital myopathy (Sanoudou and Beggs, 2001), with hallmark features that include muscle weakness and the presence of nemaline bodies in skeletal muscle fibres (North *et al*., 1997). To date, seven genes have been implicated in nemaline myopathy. Strikingly, six of these genes code for proteins of the skeletal muscle thin filament: alpha tropomyosin 3 and beta tropomyosin (*TPM3* and *TPM2*), nebulin (*NEB*), actin alpha 1 (*ACTA1*), troponin T type 1 (*TNNT1*), and cofilin 2 (*CFL2).* The seventh implicated gene, *KBTBD13*, encodes a ubiquitin ligase whose function in skeletal muscle is currently unknown (Sambuughin *et al*., 2010, 2012). With mutations in *NEB* likely accounting for >50% of nemaline myopathy cases (Pelin *et al*., 1999), *NEB* is the most frequently affected gene in nemaline myopathy. To date, 64 different mutations in *NEB* have been reported in nemaline myopathy probands (Pelin *et al*., 1999; Lehtokari *et al*., 2006, 2009).

Nebulin is a giant sarcomeric protein (~800 kDa); its C-terminus is anchored in the Z-disk and its N-terminus is located close to the thin filament pointed end. Thus, a single nebulin molecule spans nearly the entire length of the thin filament (Fig. 1). Insights into the role of nebulin's functions made a leap forward when two full nebulin knockout mouse models were published (Bang *et al*., 2006; Witt *et al*., 2006). Nebulin plays important roles in sarcomeric structure and contractile performance. It stabilizes the thin filament and specifies its minimal length (Bang *et al*., 2006; Witt *et al*., 2006; Castillo *et al*., 2009; Gokhin *et al*., 2009; Pappas *et al*., 2010). Recent evidence also suggests that nebulin modulates both the kinetics of actomyosin interaction (Bang *et al*., 2009; Chandra *et al*., 2009) and the calcium sensitivity of force generation (Chandra *et al*., 2009). Skeletal muscle fibres of patients with nemaline myopathy with *NEB* mutations might develop muscle weakness due to loss of these functions of nebulin; their myofibres contain shorter thin filaments (Ottenheijm *et al*., 2009*b*), have altered crossbridge cycling kinetics (Ottenheijm *et al*., 2010; Lawlor *et al*., 2011; Ochala *et al*., 2011), and their calcium-sensitivity of force generation is reduced (Ottenheijm *et al*., 2010). However, studies on muscle fibres from patients are limited due to, for example, the small size of diagnostic muscle biopsies and the heterogeneity of the study populations. Consequently, our understanding of the mechanisms underlying muscle weakness in patients with nemaline myopathy with nebulin mutations remains incomplete. To improve this understanding requires the development of mouse models that harbour mutations in *Neb* that are found in patients.

Here, we have generated a mouse in which *Neb* exon 55 is deleted (Fig. 1)—an in-frame deletion—to model a founder mutation frequently seen in patients with nemaline myopathy and which causes autosomal recessive nemaline myopathy (Anderson *et al*., 2004; Lehtokari *et al*., 2006, 2009). This model ($Neb^{\Delta Exon55}$) allowed, for the first time, for a detailed and comprehensive investigation of the disease mechanisms caused by a nebulin mutation and for the evaluation of potential treatments. Our findings reveal that homozygous mice have a phenotype that recapitulates important features observed previously in patients with nemaline myopathy with deletion of *NEB* exon 55, including severe muscle weakness and, importantly we show that muscle strength can be restored by a novel fast skeletal troponin activator that, at submaximal force levels, augments the response of the thin filament to calcium.

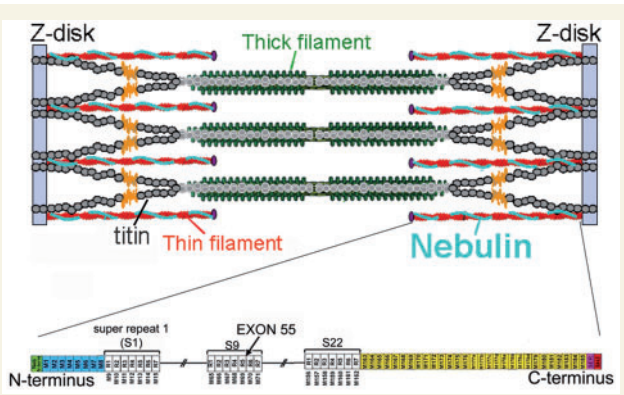

Figure 1 *Top*: Schematic of the location of nebulin in the sarcomere. *Bottom*: Schematic of the nebulin protein. Nebulin has a highly modular structure, within the central region (M9-M162) seven modular repeats arranged into 22 super-repeats. Exon 55 codes for 35 amino acids that are part of repeat 5 and 6 (super-repeat 9). Note that exon 55 in the human and murine nebulin gene are equivalent.

Materials and methods

Generation of $Neb^{\Delta Exon55}$ mice

$Neb^{\Delta Exon55}$ mice were designed to mimic the 2502-bp deletion that has previously been found to cause nemaline myopathy in humans (Anderson *et al*., 2004). Note that *Neb* exon 55 is the murine equivalent of the exon deleted in human patients (Kazmierski *et al*., 2003). The construct replaced exon 55 and parts of introns 54 and 55 with a flippase recognition target (FRT) flanked neomycin cassette. No differences in phenotype (life-span, body weight, and nebulin protein levels) were found when the neomycin cassette was removed with a flippase (FLP) deleter strain [B6; SJL-Tg(ACTFLPe)9205Dym/J- purchased from Jackson Laboratories]. Animals were maintained on a C57/BL6 background. All experiments were approved by IACUC and followed the NIH Guidelines 'Using Animals in Intramural Research' for animal use.

A targeting construct was assembled by cloning arms of homology from C57/BL6 genomic DNA (purchased from Jackson Labs) into a pCKOB vector. The vector was introduced into C57BL/6J-$Tyr^{c\text{-}2J}$/J embryonic stem cells by electroporation. The deletion was introduced by homologous recombination and selected by negative selection against thymidine kinase (using Ganciclovir) and positive selection for neomyosin resistance (G418). The surviving embryonic stem cell clones were verified by long PCR using primers (P1) 5′-ATTGACAATGCCGATTAACTACTGC-3′ and (P2) 5′-CTGGCACTC TGTCGATACCC-3′ (left arm) (P3) 5′-ACACGCGTCACCTTAATATG C-3′ and (P4) 5′-CCCAGCTGCTTACGGTAGCC-3′ and used to produce $Neb^{\Delta Ex55}$ mice by injection into C57/BL6 blastocyst. Genotyping was performed using tail digests using GoTaq® Green Master Mix (Promega). The following primer sets were used: (P5)-reverse 5′-GAAAGGAACTCTGTCCTCTGG-3′; (P6) WT forward

5′-GCATTCTTGCTCTTTCTTGTATGG-3′; (P3) *Neb*$^{\Delta Ex55}$ forward 5′-ACACGCGTCACCTTAATATGC-3′; (P7) *Neb*$^{\Delta Ex55}$ neo removed forward 5′-ACACCCAGGCAGAAGCTAGG-3′.

Histochemistry and electron microscopy

Cross sections (5 μm) of isopentane-frozen quadriceps muscles were taken midway down the length of the muscle and stained with haematoxylin and eosin or Gomori trichrome using standard histochemical techniques. For Gomori trichrome staining, sections were stained in Harris haematoxylin (Richard Allen Scientific) for 5 min, rinsed, and then stained in Gomori One-Step Light Green Solution (Newcomer Supply) for 10 min. Following an additional rinse and differentiation in 0.2% acetic acid (Newcomer Supply) for 2 min, sections were dehydrated and coverslipped using standard techniques. Light microscopic images were captured using an Olympus DP72 camera and cellSens Standard software (Olympus). For the determination of fibre size in quadriceps muscle sections, immunofluorescence was performed using anti-dystrophin antibodies, and a representative area of the muscle was photographed using a Zeiss ImagerZ1 microscope with an Axiocam HRC camera. The minFeret diameter (the smallest diameter across the myofibre) was measured manually in sections from four wild-type mice (range 653 to 862 fibres measured) and three *Neb*$^{\Delta Exon55}$ mice (range 1003 to 1343 fibres measured) using Zeiss Axiovision 4.8 software. For electron microscopy, glutaraldehyde-fixed portions of tibialis cranialis muscle were submitted to the Microbiology and Molecular Genetic Electron Microscopy Facility at the Medical College of Wisconsin. Tissue was then fixed in 2.5% glutaraldehyde in 0.1 M cacodylate buffer pH 7.4 for 60 min, washed 3 × 10 min in 0.1 M cacodylate buffer, post-fixed with 1% potassium ferrocyanide reduced OsO_4 for 3 h on ice, dehydrated through graded methanol, and embedded in EMbed 812 resin (hard). Ultrathin sections (60 nm) were contrasted with uranyl acetate and lead citrate and viewed in a Hitachi H600 TEM.

Gel electrophoresis and western blotting

Gel electrophoresis of nebulin was with 1% agarose gels and has been described in detail previously (Warren *et al*., 2003). Muscle samples from 20 wild-type and 20 *Neb*$^{\Delta Exon55}$ mice were flash frozen in liquid nitrogen after dissection. Samples were pulverized to a fine powder, solubilized and loaded on 1% agarose gels. Gels were then stained with Coomassie blue and scanned using an Epson expressions scanner.

For western blots, samples were loaded in 0.8% SDS-agarose gels and run at 15 mA/gel for 3 h. Gels were transferred onto 0.45 μm polyvinylidene fluoride membranes (Imobilon) using a Bio-Rad semi-dry transfer unit at 152 mA/gel for 2.5 h. Blots were stained using Ponceau S to visualize total protein, dried and imaged. Blots were then rehydrated, blocked with 50% Odyssey Blocking Buffer in PBS for 1 h and incubated with Rabbit anti-nebulin N-terminus (Myomedix) overnight. Primary antibody was then removed and CF680 goat anti-rabbit secondary (Biotium Inc.) was added. Blots were scanned and analysed using an Odyssey infrared imaging system (Li-Cor Biosciences).

Nebulin transcriptional profiling

Day 4 longissimus dorsi muscle was isolated from wild-type and *Neb*$^{\Delta Ex55}$ mice and stored in RNAlater (Ambion). RNA was isolated using RNeasy® Fibrous Tissue Mini Kit (Qiagen). A custom microarray was prepared by spotting 50-mer oligonucleotides in triplicate onto GAPSII amino-silane coated slides (Corning) with a robotic arrayer (Virtek). Oligonucleotide sequences for every murine nebulin exon were selected with 45–55% GC content, T_m near 70°C, low self-complementarity, and specificity based on NCBI BLAST searches with no off-target stretches longer than 25 nt with identity greater than 80%; for exons shorter than 50 nt the selected sequence spans an exon–exon junction. Sequence-specificity was confirmed by BLAT against the current mouse genome (GRCm38/mm10). For optimizing hybridization conditions, 5 bp mismatch controls were incorporated. The array had been validated by analysing transcripts isolated from human muscle with known nebulin exon composition. RNA was reverse transcribed and amplified using SenseAmp (Genisphere), and SuperScript® III (Invitrogen) and dye-coupled with Alexa Fluor® 555 or AlexaFluor 647 (Invitrogen). Sample pairs were hybridized with SlideHyb™ Glass Array Hybridization Buffer #1 (Ambion) in a GeneTAC Hybridization Station (Genomic Solutions); slides were scanned with an ArrayWoRX scanner and the results analysed using the R package CARMA (Greer *et al*., 2006).

Immunofluorescence confocal scanning laser microscopy

Small muscle strips were dissected and permeabilized overnight at ~4°C in relaxing solution (in mM; 20 BES, 10 EGTA, 6.56 $MgCl_2$, 5.88 NaATP, 1 DTT, 46.35 K-propionate, 15 creatine phosphate, pH 7.0 at 20°C) containing 1% (v/v) Triton™ X-100. Immunolabelling and confocal scanning laser microscopy was performed as described previously (Ottenheijm *et al*., 2009*b*). Primary antibodies: anti-α-actinin (mouse monoclonal, A7811, Sigma-Aldrich), anti-tropomodulin-1 (Witt *et al*., 2006) Alexa Fluor® 488 conjugated phalloidin (A12379, Invitrogen), anti-CapZα (mouse monoclonal, 5B12.3, DSHB), and rabbit anti-nebulin N-terminus (Myomedix). Secondary antibodies: Alexa Fluor® 594 (goat anti-mouse, Invitrogen), and Alexa Fluor® 488 (goat anti-rabbit, Invitrogen). Secondary antibodies did not stain when used without primary antibodies (data not shown). Images were produced using a Bio-Rad MRC 1024 confocal laser scanning microscope with the LaserSHARP 2000 software package (Hercules). From the acquired images, thin filament lengths were determined using ImageJ software (National Institutes of Health).

Permeabilized fibre contractility

For contractility experiments we used tibialis cranialis muscle; the equivalent of m. tibialis anterior in humans, which has been shown to be selectively affected in patients with nemaline myopathy with nebulin mutations (Jungbluth *et al*., 2004). The procedures for permeabilized muscle fibre contractility were as described previously (Ottenheijm *et al*., 2009*a*, *b*, 2010, 2011), with minor modifications. In short, small strips dissected from muscle from six wild-type and six *Neb*$^{\Delta Exon55}$ mice were permeabilized, or skinned, overnight at ~4°C in relaxing solution (in mM; 20 BES, 10 EGTA, 6.56 $MgCl_2$, 5.88 NaATP, 1 DTT, 46.35 K-propionate, 15 creatine phosphate, pH 7.0 at 20°C) containing 1% (v/v) Triton™ X-100. The skinning procedure renders the membranous structures in the muscle fibres permeable, which enables activation of the myofilaments with exogenous Ca^{2+}. Preparations were washed thoroughly with relaxing solution and stored in 50% glycerol/relaxing solution at −20°C. Small muscle fibre bundles (diameter ~0.07 mm) were dissected from the permeabilized strips, and were attached to a strain gauge and a high-speed motor using aluminium foil clips. Experiments were performed at 20°C.

The XY (width) and XZ (depth, using a prism) dimensions of bundle diameters were measured with a ×40 objective. The muscle bundle cross-sectional area was calculated from the average of three width and depth measurements made along the length of the muscle bundle. The preparation was activated at pCa 4.5 (pCa = −log of molar free Ca^{2+} concentration) to obtain maximal Ca^{2+}-activated force. Maximal tension was determined by dividing the force generated at pCa 4.5 by cross-sectional area. To determine force–sarcomere length relations, the maximal force generated at various sarcomere lengths was determined. Sarcomere length was measured with an on-line laser-diffraction system (Granzier and Wang, 1993).

To determine the force–pCa relation, muscle preparations were sequentially bathed in solutions with pCa values ranging from 4.5 to 9.0 and the steady-state force was measured. Measured force values were normalized to the maximal force obtained at pCa 4.5. The obtained force–pCa data were fit to the Hill equation, providing pCa_{50} (pCa giving 50% maximal active tension) and the Hill coefficient, n_H, an index of myofilament cooperativity.

To determine a dose-response curve for the fast skeletal troponin activator CK-2066260 (Cytokinetics Inc) tissue was exposed to pCa solutions of 6.25 with increasing concentrations (1, 2, 5, 10 and 20 μM) of CK-2066260 dissolved in 1% dimethylsulphoxide (DMSO) as vehicle. Note that 1% DMSO did not affect muscle fibre contractility (data not shown). CK-2066260 enhanced submaximal force generation with a maximal effect at 5 μM (data not shown), which is in accordance with previously reported dose-response curves of its analogue CK-2017357 (Russell *et al*., 2012). Accordingly, experiments were conducted with either CK-2066260 (5 μM) or vehicle alone (1% DMSO). Force–pCa relations were determined as described above.

To measure the rate of tension redevelopment (k_{tr}), we used the large slack/release approach (Brenner and Eisenberg, 1986), to disengage force generating crossbridges from the thin filaments, which were isometrically activated. Three different bathing solutions were used during the experimental protocols: a relaxing solution, a pre-activating solution with low EGTA (ethylene glycol tetraacetic acid) concentration, and an activating solution. The composition of these solutions was as described previously (Stienen *et al*., 1996). Fast activation of the fibres was achieved by transferring the permeabilized fibres from the pre-activation solution containing a low concentration of EGTA (pCa 9.0) to a pCa 4.5 activating solution. Once the steady-state was reached, a slack equivalent to 10% of the muscle length was rapidly induced at one end of the muscle using the motor. This was followed immediately by an unloaded shortening lasting 30 ms. The remaining bound cross-bridges were mechanically detached by rapidly (1 ms) restretching the muscle fibre to its original length, after which tension redevelops. The rate constant of monoexponential tension redevelopment (k_{tr}) was determined by fitting the rise of tension to the following equation: $F = F_{ss}(1 - e^{-ktr.t})$, where F is force at time t and k_{tr} is the rate constant of tension redevelopment.

To determine force simultaneously with ATP consumption rate, we used the system described by Stienen *et al*. (1996). To measure the ATPase activity, a near UV light was projected through the quartz window of the bath (30 μl volume and temperature controlled at 20°C) and detected at 340 nm. The maximum activation buffer (pCa 4.5) contained 10 mM phosphoenol pyruvate, with 4 mg/ml pyruvate kinase (500 U/mg), 0.24 mg/ml lactate dehydrogenase (870 U/mg) and 20 μM diadenosine-5′ pentaphosphate (A_2P_5). For efficient mixing, the solution in the bath was continuously stirred by means of motor-driven vibration of a membrane positioned at the base of the bath. ATPase activity of the permeabilized fibre bundles was measured as follows: ATP regeneration from ADP is coupled to the breakdown of phosphoenol pyruvate to pyruvate and ATP catalysed by pyruvate kinase, which is linked to the synthesis of lactate catalysed by lactate dehydrogenase. The breakdown of NADH, which is proportional to the amount of ATP consumed, is measured online by UV absorbance at 340 nm. The ratio of light intensity at 340 nm (sensitive to NADH concentration), and the light intensity at 410 nm (reference signal), is obtained by means of an analogue divider. After each recording, the UV absorbance signal of NADH was calibrated by multiple rapid injections of 0.25 nmol ADP (0.025 μl of 10 mM ADP) into the bathing solution, with a stepper motor-controlled injector. The slope of the [NADH] versus time trace during steady-state tension development of a calcium-induced contraction (Fig. 8B) was determined from a linear fit and the value divided by the fibre volume (in mm^3) to determine the fibre's ATPase rate. ATPase rates were corrected for the basal ATPase measured in relaxing solution. The ATPase rate was divided by tension (force/cross-sectional area) to determine the tension cost.

Myofibril contractility

Myofibrils were prepared from flash frozen and then thawed tibialis cranialis muscles from 4–7 day old wild-type ($n = 5$) and and homozygous $Neb^{\Delta Exon55}$ ($n = 5$) mice, and placed in ice-cold rigor solution containing (mM): NaCl 132, KCl 5, MgCl2 1, Tris 10, EGTA 5 (pH 7.1). The muscles were incubated for 3 h in the same solution with 1% Triton™-100. Triton was then removed and the muscles sheared in rigor solution to produce myofibril suspensions. In the present experiments we used previously published techniques (Tesi *et al*., 2002). Briefly, to study myofibrillar force development a small volume of the myofibril suspension was transferred to a temperature-controlled chamber (15°C) filled with relaxing solution (pCa 8.0) and mounted on an inverted microscope. Single myofibrils or bundles of few myofibrils (25–80 μm long, 1–4 μm wide) were mounted horizontally between two glass microtools. One tool was connected to a length-control motor that could produce rapid (<1 ms) length changes. The second tool was a calibrated cantilevered force probe (2–6 nm/nN; frequency response 2–5 kHz). Force was measured from the deflection of the image of the force probe projected on a split photodiode. Average sarcomere length and myofibril diameter were measured from image analysis. The initial sarcomere length of the preparations was adjusted to ~2.2 μm. Myofibrils were activated and relaxed by rapidly translating the interface between two flowing streams of different pCa solutions across the length of the preparation. The solution change took place with a time constant of 2–3 ms and was complete in <5 ms. Activating and relaxing solutions, calculated as previously described (Tesi *et al*., 2002), were at pH 7.0 and contained 10 mM total EGTA (CaEGTA/EGTA ratio set to obtain pCa 8.0 and 4.5), 5 mM MgATP, 1 mM free Mg^{2+}, 10 mM MOPS, propionate and sulphate to adjust the final solution to an ionic strength of 200 mM and monovalent cation concentration of 155 mM. Creatine phosphate (10 mM) and creatine kinase (200 U/ml) were added to all solutions. Contaminant inorganic phosphate (Pi) from spontaneous breakdown of MgATP and creatine phosphate was reduced to <5 μM by an inorganic phosphate scavenging system (purine-nucleoside-phosphorylase with substrate 7-methyl-guanosine). All solutions to which the muscles and myofibrils were exposed contained a cocktail of protease inhibitors including leupeptin (10 μM), pepstatin (5 μM), PMSF (200 μM) and E64 (10 μM), as well as NaN_3 (500 μM) and DTE (2 mM).

Statistical analyses

Data are presented as mean ± SEM. For statistical analyses, *t*-tests were used. The effect of CK-2066260 was investigated within

individual muscle fibre preparations; a paired *t*-test was performed in these analyses. $P < 0.05$ was considered to be statistically significant.

Results

$Neb^{\Delta Exon55}$ mice display a phenotype that resembles nemaline myopathy

Using homologous recombination, we removed exon 55 from the nebulin gene. Mice heterozygous for the targeted allele are viable and fertile and survive into adulthood with no obvious clinical or contractile phenotype. Homozygous offspring (referred to as $Neb^{\Delta Exon55}$) are produced at expected Mendelian genetic ratios (~1/4 of total number of pups using heterozygous breedings, Fig. 2A), with a weight at birth that is not different from that of heterozygous and wild-type littermates. However, $Neb^{\Delta Exon55}$ mice show severe growth retardation after birth (Fig. 2B) and typically do not survive past the first week (Fig. 2C).

Nemaline myopathy in humans is characterized by the presence of nemaline bodies (often called nemaline rods when they are rod-shaped), which is often accompanied by myofibre hypotrophy. To test whether these histological characteristics of nemaline myopathy are present in $Neb^{\Delta Exon55}$ mice, we first evaluated sections of quadriceps muscle stained with haematoxylin and eosin or Gomori trichrome. As shown in Fig. 3A, the haematoxylin and eosin stained sections from 6-day-old wild-type and $Neb^{\Delta Exon55}$ mice reveal smaller muscle fibres in $Neb^{\Delta Exon55}$ mice. Quantitative analysis revealed that where average fibre minFeret diameter was $13.0 \pm 0.4\,\mu m$ in wild-type mice; this was significantly reduced to $10.1 \pm 0.3\,\mu m$ in $Neb^{\Delta Exon55}$ mice ($P < 0.01$). Discrete populations of large and small fibres were not observed in $Neb^{\Delta Exon55}$ mouse muscle. The number of central nuclei was <1% in both wild-type and $Neb^{\Delta Exon55}$ muscle, and $Neb^{\Delta Exon55}$ muscle showed no signs of fibrosis. Nemaline bodies were not visible at the light microscopic level on Gomori trichrome stain (Fig. 3A, lower panel)

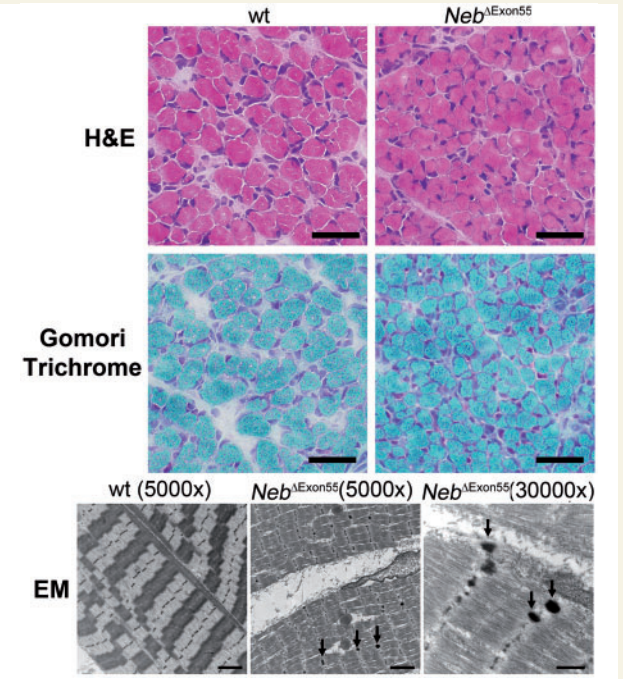

Figure 3 Histological findings in 6-day-old wild-type and $Neb^{\Delta Exon55}$ mice. Haematoxylin and eosin (H&E) stained sections of quadriceps muscle from wild-type (wt) and $Neb^{\Delta Exon55}$ mice reveal smaller muscle fibres in $Neb^{\Delta Exon55}$ mice. Nemaline rods were not visible at the light microscopic level on Gomori trichrome stain, but electron-dense nemaline bodies (arrows) were seen on electron microscopy (EM) in the tibialis cranialis muscle from all $Neb^{\Delta Exon55}$ mice. Nemaline bodies were not seen in wild-type mouse muscle. Scale bar = 40 μm for haematoxylin and eosin and Gomori trichrome images, 2 μm for ×5000 electron microscopy images, and 500 nm for the ×30 000 electron microscopy image.

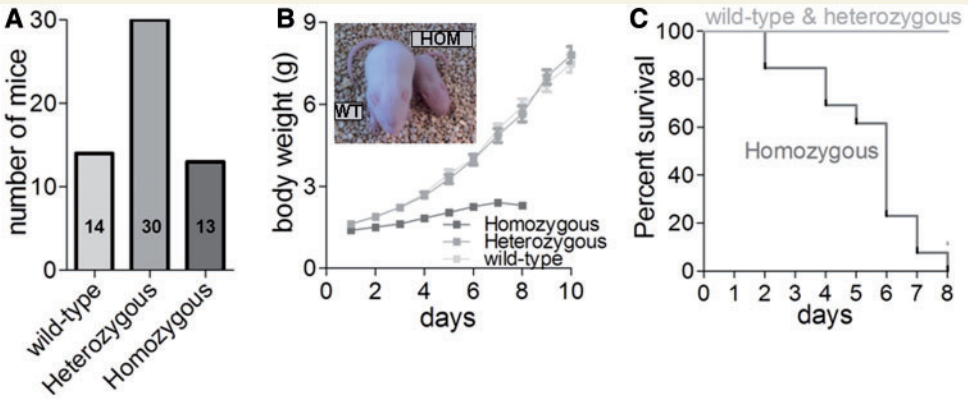

Figure 2 (**A**) Homozygous ($Neb^{\Delta Exon55}$) mice are born close to Medelian ratio: 13 homozygous mice out of total 57 pups when using heterozygous breedings. (**B**) Body weight of $Neb^{\Delta Exon55}$ mice at birth is not different from that of HET and wild-type (WT) littermates. $Neb^{\Delta Exon55}$ mice show severe growth retardation after birth, and (**C**) typically do not survive past the first week (survival curve based on 57 pups). *Inset*: Photograph of a $Neb^{\Delta Exon55}$ (HOM) and a wild-type littermate mouse illustrating the growth retardation in $Neb^{\Delta Exon55}$ mice.

of quadriceps muscle, but electron microscopy revealed electron-dense nemaline bodies at the location of the Z-band (arrows, Fig. 3B) in the tibialis cranialis (the murine equivalent of tibialis anterior in humans) muscles of $Neb^{\Delta Exon55}$ mice. These nemaline bodies displayed electron density equivalent to normal Z-bands, which differentiates them from the Z-band streaming that can be found in a variety of muscle disorders. Nemaline bodies were not seen in wild-type mouse muscle. Thus, $Neb^{\Delta Exon55}$ mice display a histological phenotype that resembles nemaline myopathy, including the presence of nemaline bodies and hypotrophic fibres.

Deletion of exon 55 results in severely reduced nebulin protein levels

NEB exon 55 encodes 35 amino acids and represents ~4 kDa at the protein level. As deletion of exon 55 maintains the reading frame 3′ of exon 55, we expected the $Neb^{\Delta Exon55}$ mice to express a nebulin isoform that is ~4 kDa smaller than wild-type nebulin. However, SDS-agarose gel analysis showed that, in 5-day-old $Neb^{\Delta Exon55}$ mice, nebulin proteins levels were severely reduced in all muscle types tested (Fig. 4A). Western blot experiments using an antibody directed against the nebulin N-terminus confirmed these findings (Fig. 4B). To evaluate whether the low nebulin protein levels at Day 5 after birth were preceded by a gradual decrease from normal levels at birth, we also evaluated nebulin levels at Day 1 after birth (Fig. 4C) and at embryonic Day 19 (Fig. 4D). These experiments showed that nebulin protein levels were severely reduced in $Neb^{\Delta Exon55}$ muscle at both time points. Nebulin protein levels in $Neb^{\Delta Exon55}$ quadriceps muscle (normalized to myosin heavy chain) was ~10% of wild-type values in embryonic Day 19 tissue, 8% of wild-type values in post-natal Day 1 tissue, and decreased to ~2% of wild-type values in post-natal Day 5 tissue (Fig. 4E). Thus, deletion of exon 55 results in severly reduced nebulin protein levels.

To evaluate whether the reduced nebulin protein levels were caused by alterations at the level of DNA transcription or of messenger RNA translation, we used a homemade nebulin exon microarray to test which of the 166 murine nebulin exons are included in the full-length nebulin messenger RNA. As shown in Fig. 5, in addition to the expected reduction of exon 55 messenger RNA, transcription of nearly all nebulin exons was significantly reduced in $Neb^{\Delta Exon55}$ muscle. Thus, these results suggest that the low nebulin protein levels in $Neb^{\Delta Exon55}$ mice are not caused by defects in the translation of nebulin messenger RNA into protein but rather by changes in transcription of the mutant nebulin gene or in the stability of the mutant nebulin messenger RNA.

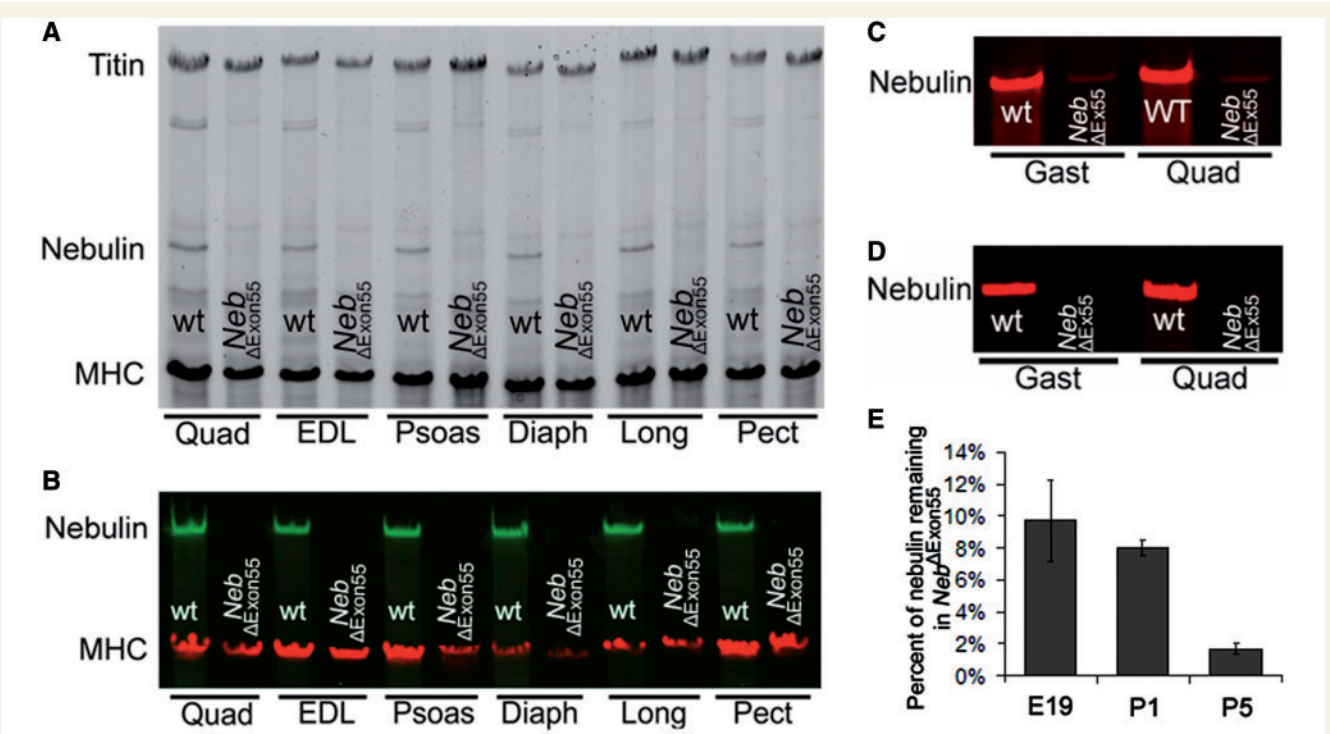

Figure 4 (**A**) SDS-agarose gel electrophoresis reveals severely reduced nebulin protein levels in $Neb^{\Delta Exon55}$ mice in all skeletal muscle types tested, whereas myosin heavy chain (MHC) and titin levels are unaltered. Muscles are obtained from 5-day-old mice. (**B**) Quantitative western blotting studies with an antibody against nebulin's N-terminus shows that nebulin protein levels are ~2% of wild-type (wt) levels. Western blotting studies with the same antibody on muscle from embryonic Day 19 (E19) mice (**C**) and 1-day-old (P1) mice (**D**) and show that nebulin protein is 10% of wild-type values at Day 19 (E19) and 8% of wild-type values at Day 1 (**E**). *$P < 0.05$. Quad = m. quadriceps; EDL = extensor digitorum longus; Psoas = m. psoas major; Diaph = m. diaphragm; Long = m. longissimus dorsi; Pect = m. pectoralis major; Gast = m. gastrocnemius.

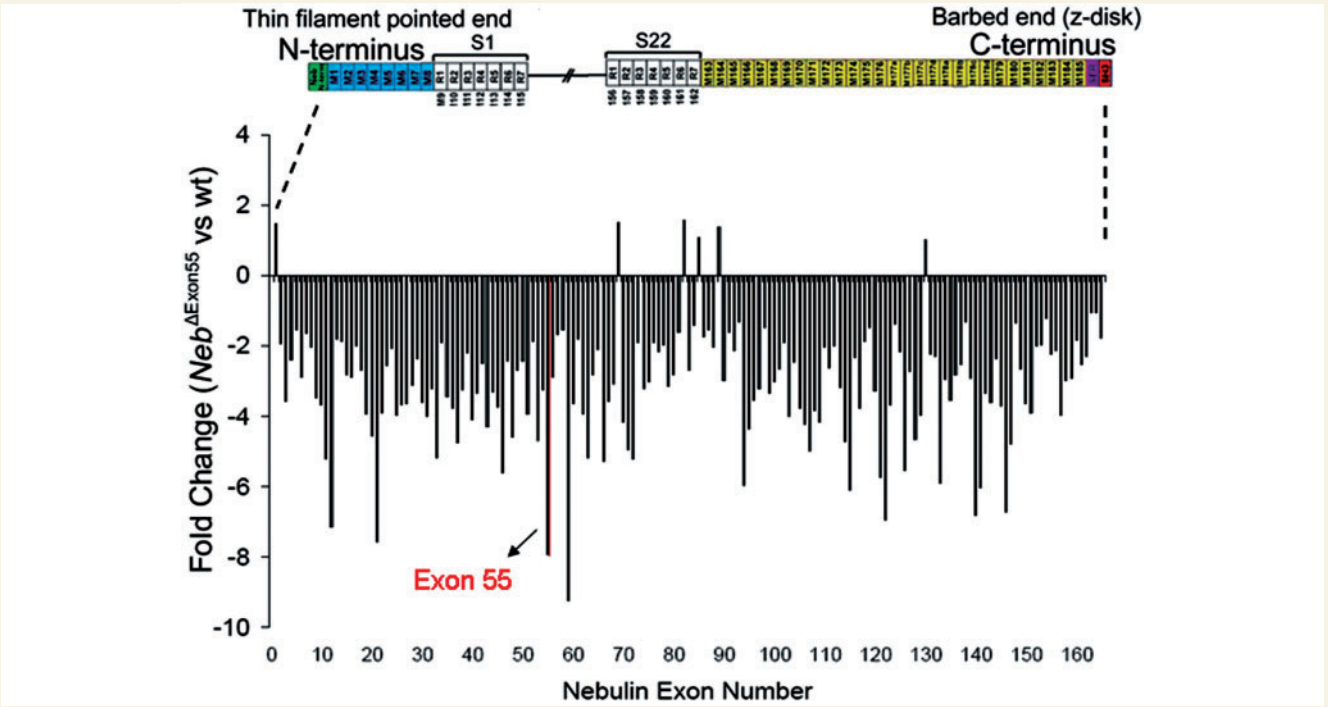

Figure 5 Microarray-based gene expression analysis of nebulin exon expression of m. longissimus dorsi in $Neb^{\Delta Exon55}$ mice compared with wild-type (wt) mice at 4 days of age. The array contains all 166 murine nebulin exons. Nearly all nebulin exons are downregulated in $Neb^{\Delta Exon55}$ mice.

$Neb^{\Delta Exon55}$ mice have shorter thin filament lengths

Nebulin plays an important role in specifying thin filament length, and shorter thin filaments clearly contribute to reduced sarcomeric force generation in human nebulin-deficient nemaline myopathy (Ottenheijm *et al*., 2009*b*). Therefore, we measured thin filament length in $Neb^{\Delta Exon55}$ muscle fibres. Using immunofluorescence confocal scanning laser microscopy we determined the location of tropomodulin (a thin filament pointed end capping protein) relative to the Z-disk and we measured the width of the band obtained using the fluorescently labelled actin-binding protein phalloidin.

Figure 6A shows that the staining pattern of fluorescently labelled phalloidin differed between myofibrils from $Neb^{\Delta Exon55}$ and wild-type tibialis cranialis muscle; wild-type myofibrils showed broad actin labelling with uniform intensity (except for the Z-disk area where actin filaments overlap), whereas in $Neb^{\Delta Exon55}$ myofibrils the labelling was narrower, and intensity gradually decreased from the Z-disk towards the middle of the sarcomere. Densitometric analysis revealed that the width at half-maximal intensity was $2.25 \pm 0.03\,\mu m$ for wild-type and $1.75 \pm 0.01\,\mu m$ for $Neb^{\Delta Exon55}$ myofibrils (Fig. 6A).

Tropomodulin staining in wild-type myofibrils showed a distinct doublet in the middle of the sarcomere, $2.03 \pm 0.03\,\mu m$ apart, measured across the Z-disk, whereas in myofibrils from $Neb^{\Delta Exon55}$ mice this value was only $1.67 \pm 0.03\,\mu m$ (Fig. 6B). These findings support the results from the phalloidin experiments and suggest that thin filament lengths are reduced from $\sim 1.0\,\mu m$ in wild-type myofibrils to $\sim 0.85\,\mu m$ in $Neb^{\Delta Exon55}$ myofibrils.

The experiments with fluorescently labelled tropomodulin revealed that thin filaments are shorter in $Neb^{\Delta Exon55}$ myofibrils and suggested that capping at the thin filament pointed end by tropomodulin remains intact in these myofibrils. Immunofluorescence experiments on CapZ (a thin filament barbed end capping protein) showed that capping at the barbed end also remains intact in $Neb^{\Delta Exon55}$ myofibrils (Fig. 6C).

Finally, the data in Fig. 6D, in which an antibody against nebulin's N-terminus was used, show that nebulin is nearly absent from $Neb^{\Delta Exon55}$ myofibrils, thereby confirming the western blot experiments (Fig. 4). Thus, immunofluorescence confocal microscopy experiments show that in $Neb^{\Delta Exon55}$ muscle thin filament capping is intact but that thin filament length is significantly reduced.

$Neb^{\Delta Exon55}$ mice display severe muscle weakness

Force–sarcomere length relation

Because sarcomeres generate force in proportion to thick and thin filament overlap, a well-defined thin filament length is an important determinant of muscle function. This is illustrated by the force–sarcomere length relationship, which is characterized by a force plateau at optimal filament overlap, followed by a descending limb at higher sarcomere lengths as filament overlap decreases. Shortened thin filaments will reduce thick and thin filament

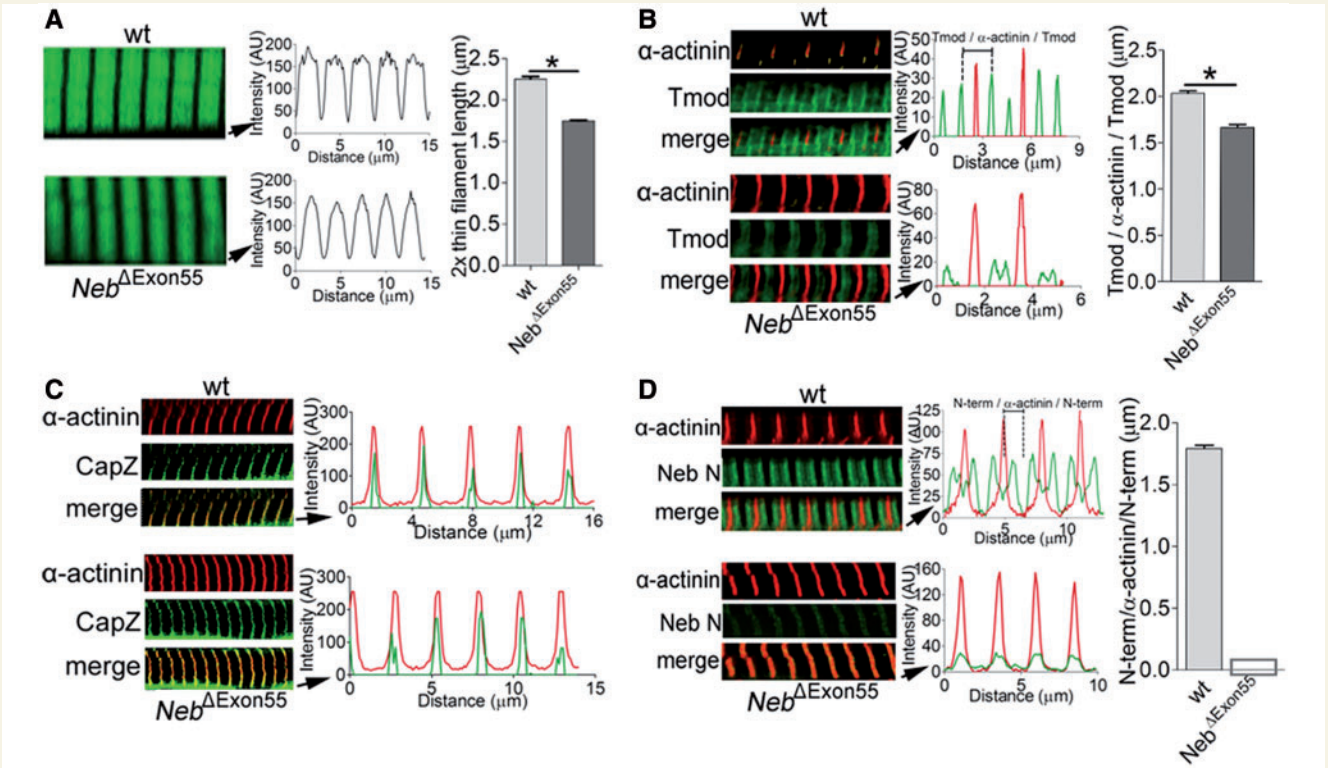

Figure 6 (**A**) *Left*: Actin staining with phalloidin-Alexa Fluor® 488 in Day 6 tibialis cranialis myofibrils from $Neb^{\Delta Exon55}$ and wild-type mice shows broad staining in wild-type myofibrils (*top*), whereas this staining is narrowed in $Neb^{\Delta Exon55}$ myofibrils (*bottom*). *Right*: Analysis of phalloidin line scan intensities revealed significantly reduced average thin filament lengths in $Neb^{\Delta Exon55}$ myofibrils. (**B**) *Left*: $Neb^{\Delta Exon55}$ and wild-type myofibrils stained for α-actinin and tropomodulin (Tmod1). *Right*: Overlay of line scan intensity profile of α-actinin and tropomodulin. The distance between tropomodulin staining (measured across the Z-disk, and indicated as Tmod-α-actinin-Tmod) is significantly reduced in $Neb^{\Delta Exon55}$ myofibrils. (**C**) CapZ staining of $Neb^{\Delta Exon55}$ and wild-type myofibrils. Staining of $Neb^{\Delta Exon55}$ myofibrils is similar to the staining pattern of wild-type myofibrils. (**D**) *Left*: Six day old $Neb^{\Delta Exon55}$ and wild-type myofibrils stained for α-actinin and nebulin's N-terminus (Neb N). *Right*: Analysis of line scan intensities. Note that Neb N staining is nearly absent in $Neb^{\Delta Exon55}$ myofibrils. $^*P < 0.05$.

overlap and impair the sarcomere's force generating capacity, which is reflected by a leftward shift of the force–sarcomere length relationship (Granzier *et al*., 1991). Hence we studied whether the reduced thin filament length in $Neb^{\Delta Exon55}$ myofibrils affects the force generating capacity of muscle by determining the force–sarcomere length relationship in permeabilized fibre preparations. Fibres from wild-type muscle showed a characteristic force plateau up to a sarcomere length of ~2.6 μm, followed by a linear descending limb (Fig. 7A). Note that the descending limb of wild-type fibres intercepts the *x*-axis at ~3.6 μm. Assuming that thick filaments are constant at ~1.6 μm, this would suggest that thin filament length is ~1.0 μm, which is in-line with thin filament lengths as determined by our confocal microscopy studies (Fig. 6A and B). Importantly, fibres from $Neb^{\Delta Exon55}$ muscle showed a leftward-shift of the force–sarcomere length relationship, indicating shorter thin filament lengths (Fig. 7A). The descending limb of $Neb^{\Delta Exon55}$ fibres intercepts the *x*-axis at a sarcomere length of ~3.4 μm, a length that is consistent with thin filament lengths of ~0.9 μm, which is close to the length as determined by the confocal microscopy studies (0.85 μm).

Considering that thin filament length is an important determinant of a muscle's force generating capacity, we also plotted tension (force normalized to fibre cross-sectional area) versus sarcomere length (Fig. 7B). Importantly, at a sarcomere length of 2.4 μm, a length on the plateau of the force–sarcomere length relation of both genotypes, absolute maximal tension was reduced in fibres from $Neb^{\Delta Exon55}$ muscle to ~38% of wild-type values (Fig. 7B). To study whether the reduced maximal tension of $Neb^{\Delta Exon55}$ fibres is caused by a reduction in myofibrillar fractional area or rather by changes in myofibrillar function, we also determined the contractile force of single myofibrils isolated from $Neb^{\Delta Exon55}$ and wild-type muscle fibres. As shown in Fig. 7C, the maximal tension generated by $Neb^{\Delta Exon55}$ myofibrils was reduced to ~36% of wild-type values, a reduction that is similar in magnitude to that observed in $Neb^{\Delta Exon55}$ fibres. Thus, these findings indicate that muscle from $Neb^{\Delta Exon55}$ mice is significantly weakened, that this weakening is primarily caused by changes in myofibrillar function, and that reduction of thin filament length contributes to weakness especially at longer sarcomere lengths.

Crossbridge cycling kinetics

Recent work has led to the notion that nebulin is important for the tuning of crossbridge cycling kinetics to maximize force generation (Chandra *et al*., 2009; Ottenheijm and Granzier, 2010). To

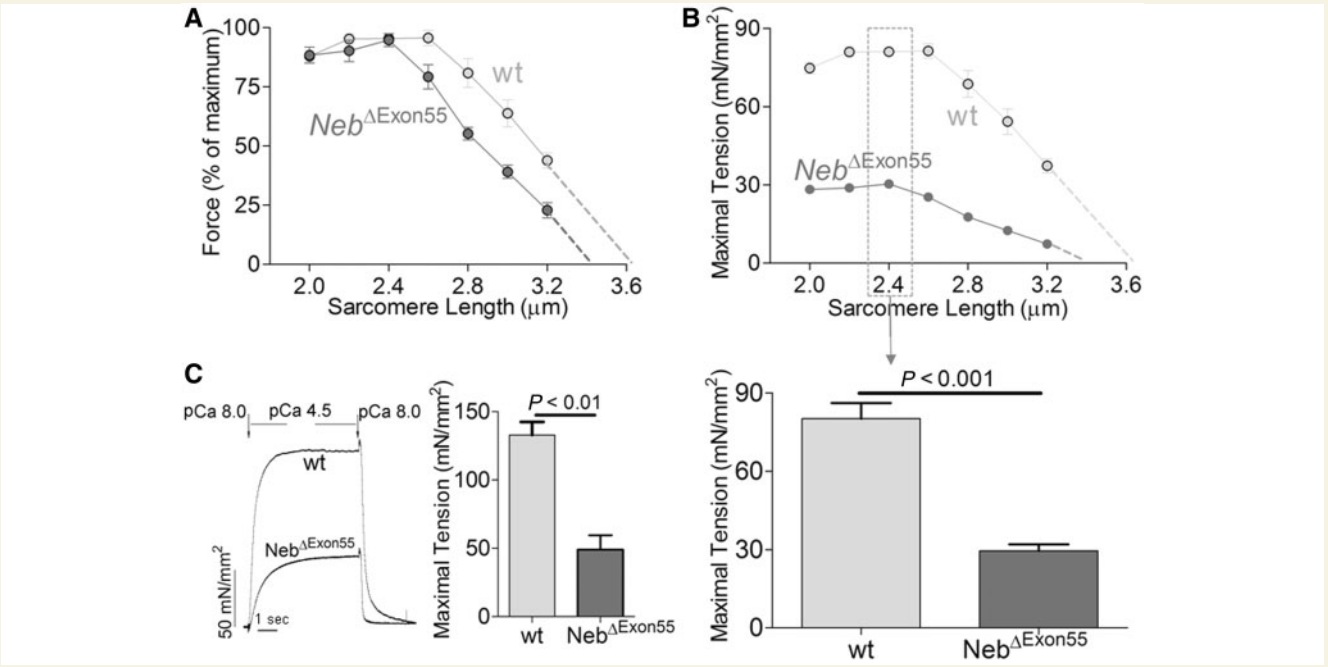

Figure 7 (**A**) The force–sarcomere length relation of tibialis cranialis fibres from 6-day-old *Neb*$^{\Delta Exon55}$ and wild-type (wt) mice, with force normalized to maximal force at the optimal length: the relation is shifted leftward in *Neb*$^{\Delta Exon55}$ fibres suggesting shorter thin filaments in *Neb*$^{\Delta Exon55}$ fibres. (**B**) *Top*: The maximal tension–sarcomere length relation of *Neb*$^{\Delta Exon55}$ and wild-type fibres, illustrating that *Neb*$^{\Delta Exon55}$ fibres develop at all sarcomere lengths a reduced level of force. This indicates that other factors, in addition to shorter thin filaments, contribute to the weakness of *Neb*$^{\Delta Exon55}$ muscle. *Bottom*: At a sarcomere length of 2.4 μm, maximal tension is reduced in fibres from *Neb*$^{\Delta Exon55}$ muscle to ~38% of wild-type values. (**C**) *Left*: Force tracing of activated single myofibrils from wild-type and *Neb*$^{\Delta Exon55}$ muscle. *Right*: Maximal tension of *Neb*$^{\Delta Exon55}$ myofibrils is reduced to ~36% of wild-type values.

determine whether changes in crossbridge cycling kinetics contribute to the weakness observed in *Neb*$^{\Delta Exon55}$ fibres, we determined the tension cost and the rate constant of force redevelopment, k_{tr}, in fibres from *Neb*$^{\Delta Exon55}$ muscle and compared results to those from wild-type muscle. To determine k_{tr}, fibres were first isometrically activated at pCa 4.5 and when a steady force was reached, crossbridges were disengaged by performing a quick release, a brief period of unloaded shortening, and then a rapid restretch to the original length. Following restretch, force rebuilds with a time course that can be fit to a monoexponential with rate constant k_{tr} (see Fig. 8A, left panel, for a typical force response). As shown in Fig. 8A, k_{tr} was significantly lower in the *Neb*$^{\Delta Exon55}$ fibres than in the wild-type fibres (4.3 ± 0.5 versus $5.9 \pm 0.3\ s^{-1}$, *Neb*$^{\Delta Exon55}$ versus wild-type, respectively). Tension cost was determined by the simultaneous measurement of the breakdown of NADH and force during contraction, with NADH levels enzymatically coupled to ATP utilization (see 'Materials and methods' section). An example of a maximally-activated *Neb*$^{\Delta Exon55}$ fibre preparation with [NADH] falling linearly during the tension plateau is shown in Fig. 8B. The slope of the [NADH] versus time curve was normalized by the fibre volume to obtain ATP consumption rates that can be compared for differently sized muscle preparations. By normalizing ATP consumption rates to the tension generated and fibre volume, the tension cost can be determined. As shown in Fig. 8B, the tension cost was significantly higher in *Neb*$^{\Delta Exon55}$ fibres compared with wild-type fibres (10.4 ± 1.1 versus 6.4 ± 0.4 pmol/mN/mm/s, *Neb*$^{\Delta Exon55}$ versus wild-type, respectively).

Next, we determined the activation and relaxation kinetics of single myofibrils isolated from *Neb*$^{\Delta Exon55}$ and wild-type muscle fibres. Due to their small size (diameter: 1–2 μm) and when combined with a rapid solution switching mechanism (Tesi *et al*., 2002) force activation and relaxation kinetics can be determined. As shown in Fig. 8C and D, the rate constants of activation (k_{act}) and of force redevelopment following a rapid-release rapid-restretch protocol (k_{tr}) were significantly reduced in *Neb*$^{\Delta Exon55}$ myofibrils; k_{act}: 1.46 ± 0.07 versus $2.89 \pm 0.21\ s^{-1}$, *Neb*$^{\Delta Exon55}$ versus wild-type, respectively; k_{tr}: 2.27 ± 0.16 versus $3.29 \pm 0.25\ s^{-1}$, *Neb*$^{\Delta Exon55}$ versus wild-type, respectively. Note that the magnitude of k_{tr} reduction in myofibrils was in the same order as observed in *Neb*$^{\Delta Exon55}$ fibres. The relaxation phase of myofibrils consists of an initial slow phase for which we determined the rate constant 'slow k_{rel}' – which is thought to reflect the apparent rate constant of detachment of force bearing crossbridges, g_{app} (tension cost is also proportional to g_{app}) (Poggesi *et al*., 2005). The subsequent fast relaxation phase is characterized by the 'fast k_{rel}'. Force relaxation kinetics in the *Neb*$^{\Delta Exon55}$ myofibrils were significantly faster than in wild-type myofibrils: slow k_{rel}: 1.17 ± 0.15 versus $0.56 \pm 0.05\ s^{-1}$, *Neb*$^{\Delta Exon55}$ versus wild-type, respectively; fast k_{rel}: 11.0 ± 1.5 versus $6.0 \pm 0.04\ s^{-1}$ *Neb*$^{\Delta Exon55}$ versus wild-type, respectively (Fig. 8D). Note that the magnitude of increase in slow k_{rel} in

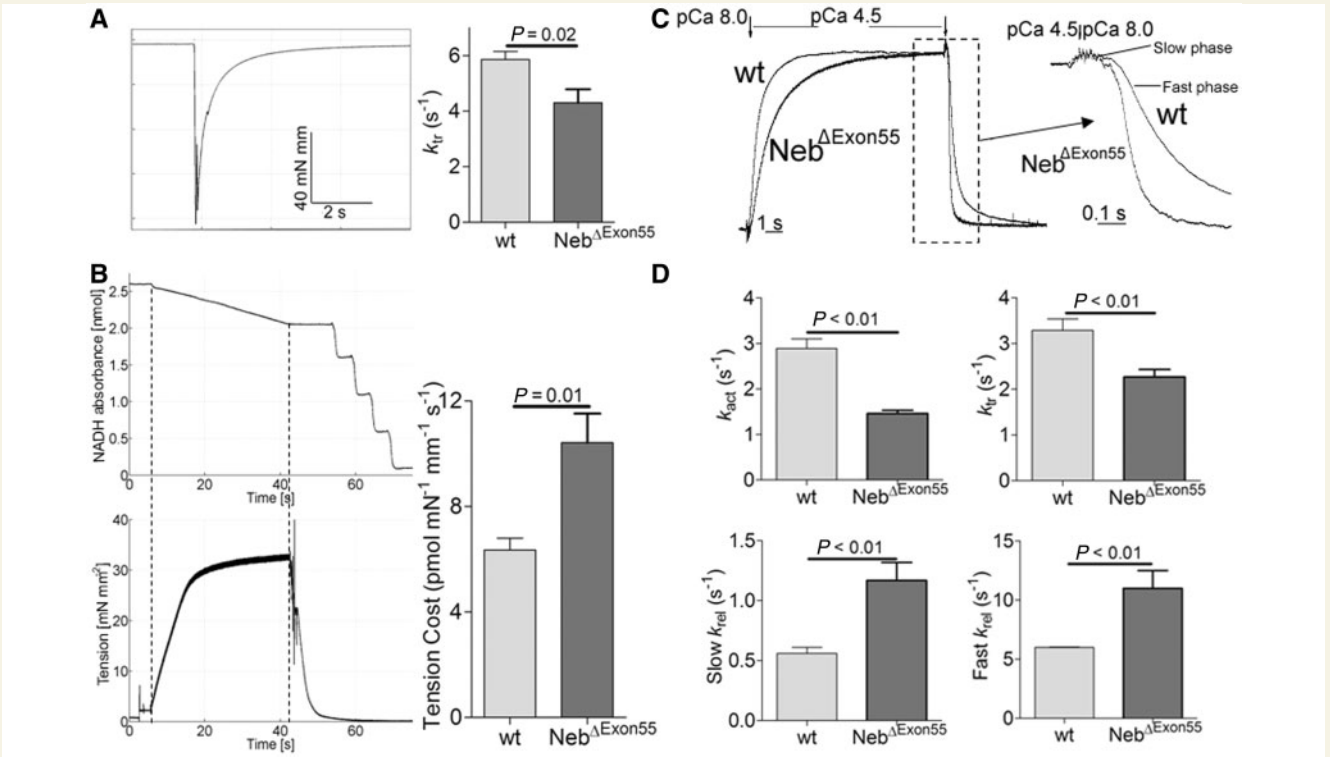

Figure 8 (**A**) k_{tr} measurements in 6-day-old *Neb*$^{\Delta Exon55}$ and wild-type (wt) fibres. *Left*: Example of a k_{tr} protocol in a *Neb*$^{\Delta Exon55}$ fibre preparation; *right*: k_{tr} is significantly lower in *Neb*$^{\Delta Exon55}$ compared with wild-type fibres. (**B**) Tension cost measurements in *Neb*$^{\Delta Exon55}$ and wild-type fibres. *Left*: Example of maximally activated *Neb*$^{\Delta Exon55}$ fibres with developed force at the bottom and [ATP] at the top. The slope of the [ATP] versus time trace was divided by fibre volume (in mm^3) to determine ATP consumption rate. ATP consumption rate was normalized to tension to determine the tension cost. *Right*: Tension cost is significantly higher in *Neb*$^{\Delta Exon55}$ compared to wild-type fibres. (**C**) An example of a protocol to determine crossbridge cycling kinetics in a myofibril. Myofibrils are rapidly activated (pCa 4.5), followed by rapid relaxation (pCa 8.0) after steady state tension is reached. From the force tracings, the rate constants of activation (k_{act}) and relaxation are determined. Relaxation consists of an initial slow phase (slow k_{rel}) followed by a fast phase (fast k_{rel}). k_{tr} is determined during a separate protocol that is similar to that applied on fibres. (**D**) Both k_{act} and k_{tr} are significantly lower in *Neb*$^{\Delta Exon55}$ compared with wild-type myofibrils, whereas slow and fast k_{rel} are significantly higher in *Neb*$^{\Delta Exon55}$ compared with wild-type myofibrils.

Neb$^{\Delta Exon55}$ myofibrils is close to that of the increase in tension cost in fibres.

Thus, these mechanical studies on both fibres and single myofibrils show that crossbridge cycling kinetics are significantly altered in muscle from *Neb*$^{\Delta Exon55}$ mice.

Calcium sensitivity of force

The calcium sensitivity of force generation is also an important parameter of muscle function as it reflects the response of force to submaximal activation levels, levels at which muscle typically operates *in vivo*. To determine the calcium sensitivity of force, permeabilized fibres from tibialis cranialis muscle were exposed to incremental calcium concentrations and the force response was recorded. As shown in Fig. 9A, the force–pCa curve of *Neb*$^{\Delta Exon55}$ fibres was shifted rightward (reflected by a lower pCa_{50} in *Neb*$^{\Delta Exon55}$ fibres: 6.22 ± 0.02 versus 6.34 ± 0.01, *Neb*$^{\Delta Exon55}$ versus wild-type, respectively), indicating that the calcium sensitivity of force was significantly reduced in fibres from *Neb*$^{\Delta Exon55}$ mice compared to those from wild-type mice. The cooperativity of activation (n_H) was not different between groups. Thus, the calcium sensitivity of force is reduced in *Neb*$^{\Delta Exon55}$ muscle.

Next, we studied the ability of the novel compound CK-2066260 to restore the calcium sensitivity of force in *Neb*$^{\Delta Exon55}$ fibres from tibialis cranialis muscle. CK-2066260 is a recently developed skeletal muscle troponin activator that amplifies the response of the thin filament to calcium in fast skeletal muscle fibres (Russell *et al*., 2012). As shown in Fig. 9B, 5 μM of CK-2066260 induced a profound increase in the pCa_{50}, an increase that was comparable between *Neb*$^{\Delta Exon55}$ and wild-type fibres (ΔpCa_{50}: 0.26 ± 0.03 versus 0.29 ± 0.02, *Neb*$^{\Delta Exon55}$ versus wild-type, respectively). Importantly, in *Neb*$^{\Delta Exon55}$ fibres, CK-2066260 increased active tension at submaximal (Ca^{2+}) to values that exceeded those of untreated wild-type fibres (Fig. 9C). These findings show the promise of fast skeletal troponin activation in restoring muscle strength in nebulin-based nemaline myopathy.

Discussion

We generated the first mouse model for nebulin-based nemaline myopathy by targeted deletion of *Neb* exon 55. Our findings show that muscle from *Neb*$^{\Delta Exon55}$ mice is severely weakened

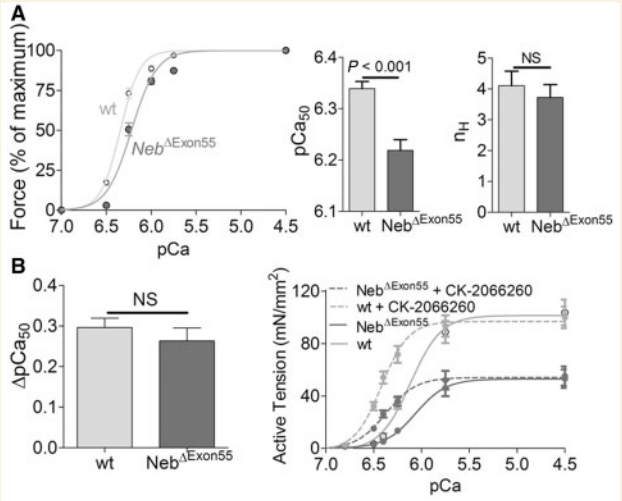

Figure 9 (**A**) Force–Ca^{2+} characteristics of tibialis cranialis fibres from 5-day-old *Neb*$^{\Delta Exon55}$ and wild-type mice. *Left*: Note the rightward shift of the force–pCa relationship in *Neb*$^{\Delta Exon55}$ compared with wild-type fibres. *Middle*: The Ca^{2+} concentration needed for 50% of maximal force generation was significantly higher (i.e. lower pCa_{50}) in *Neb*$^{\Delta Exon55}$ versus wild-type fibres, whereas no difference was found in the Hill coefficient (nH, *right*). (**B**) The effect of the fast troponin activator CK-2066260 on the force–Ca^{2+} characteristics in *Neb*$^{\Delta Exon55}$ and wild-type fibres. *Left*: 5 μM of CK-2066260 induced a large increase in the pCa_{50}, an increase that was comparable between *Neb*$^{\Delta Exon55}$ and wild-type fibres. *Right*: In *Neb*$^{\Delta Exon55}$ fibres, 5 μM CK-2066260 increased active tension at submaximal (Ca^{2+}) to values that exceeded those of untreated wild-type fibres. NS = not significant.

and contains nemaline rods, both hallmark features of nemaline myopathy. The muscle weakness in *Neb*$^{\Delta Exon55}$ mice is caused by hypotrophy of muscle fibres, and by the muscle fibres having shorter thin filaments, changes in crossbridge cycling kinetics and reduced calcium sensitivity of force generation. A novel drug that facilitates calcium binding to the thin filament significantly augmented muscle force to levels that exceed those observed in untreated control muscle. As we discuss in detail below, the overall phenotype of this new mouse model recapitulates important features observed previously in patients with nemaline myopathy with deletion of *Neb* exon 55.

Deletion of exon 55 leads to severely reduced nebulin protein levels

Nebulin is a giant protein expressed at high levels in skeletal muscle. Most of the molecule is comprised of centrally located modules (M9 to M162) that are organized into seven-module super-repeats that match the repeat of the actin filament (Fig. 1). This precise arrangement is thought to allow each nebulin module to interact with a single monomer of the actin filament (Labeit *et al*., 1991; Labeit and Kolmerer, 1995), and each nebulin super-repeat to associate with a single tropomyosin (Tm)/troponin (Tn) complex (Jin and Wang, 1991; McElhinny *et al*., 2003; Ogut *et al*., 2003). *NEB* exon 55 encodes 35 amino acids that are part of modules 69 and 70 in super-repeat 9 (Fig. 1). The absence of exon 55 in the nebulin transcript does not generate a frameshift, and the transcript is predicted to encode a protein that is 35 amino acids smaller than the normal gene product. However, as two of the encoded 35 amino acid modules of nebulin are interrupted by the deletion of exon 55, this results in the disruption of the seven-module set of super-repeat 9 (Labeit and Kolmerer, 1995). It has been proposed that this disruption causes a mismatch between nebulin and its binding sites on actin (Anderson *et al*., 2004), thereby preventing the incorporation of mutant nebulin molecules and leading to their degradation (Ottenheijm *et al*., 2009*b*). In line with this proposition, a study on five patients homozygous for deletion of *NEB* exon 55 showed that the muscle fibres of these patients have nebulin levels that are <15% of normal values (Ottenheijm *et al*., 2009*b*). The present work shows that nebulin protein was severely reduced in all muscle types tested from *Neb*$^{\Delta Exon55}$ mice, including in embryonic muscle (Fig. 4), suggesting that muscle loading after birth did not greatly accelerate the loss of nebulin protein. Hence, the proteomic phenotype of *Neb*$^{\Delta Exon55}$ mice resembles that of the full nebulin knockout models (Bang *et al*., 2006; Witt *et al*., 2006), although nebulin protein levels in the *Neb*$^{\Delta Exon55}$ mice are slightly higher and more similar to those observed in patients (Ottenheijm *et al*., 2009*b*). The nebulin exon microarray studies (Fig. 5) revealed the down-regulation of nearly all nebulin exons at the RNA level, not only exon 55. Thus, the low nebulin protein levels appear to be caused by defects at the transcript level, rather than by degradation of mutant nebulin protein. The mechanisms underlying the more severe reduction of nebulin levels in *Neb*$^{\Delta Exon55}$ mice compared to humans with the same mutation is unclear. An explanation could be that most patients with *NEB* exon 55 deletion also have very little nebulin protein and that they die *in utero*. However, the rate of miscarriage in the families that carry the *NEB* exon 55 mutation appears to be within the normal range (Beggs *et al*., in preparation) making this explanation unlikely. Alternatively, nebulin isoform composition might play a role: if inclusion of exon 55 is mandatory in the mouse and less so in humans, then this would more severely affect nebulin protein levels in *Neb*$^{\Delta Exon55}$ mice. Transcript studies in the mouse showed no differential splicing of exon 55 (Buck *et al*., 2010), consistent with the absence of nebulin expression in any of the muscle types that we studied (Fig. 4A and B). Thus if alternative splicing of human nebulin transcripts were to occur that can produce some functional nebulin isoforms devoid exon 55, this could explain why nebulin levels in *Neb*$^{\Delta Exon55}$ mice are more severely reduced than in humans with the same mutation.

Severe weakness of muscle fibres caused by thin filament dysfunction

A hallmark feature of patients with nemaline myopathy is muscle weakness, greatly affecting daily life activities and negatively impacting the quality of life (North *et al*., 1997). At the structural level, nemaline myopathy is characterized by myofibrillar disarray

originating from the Z-disk and culminating in nemaline rods, which consist of thin filament and Z-disk proteins (Engel and Gomez, 1967; Yamaguchi *et al*., 1978, 1982; Morris *et al*., 1990; North, *et al*., 1997; Sanoudou and Beggs, 2001). Importantly, the number of nemaline rods in muscle biopsies does not correlate with muscle weakness in patients with nemaline myopathy (Shimomura and Nonaka, 1989; Ryan *et al*., 2003). This suggests that myofibrillar disarray and nemaline rods are a secondary phenotype and are not the sole contributors to the muscle weakness associated with nemaline myopathy. The $Neb^{\Delta Exon55}$ model has a relative paucity of rod bodies yet muscle weakness is severe, supporting the notion that muscle weakness in nemaline myopathy with nebulin mutations is caused primarily by changes in myofilament function.

The maximal tension generated by muscle fibres from $Neb^{\Delta Exon55}$ mice was severely reduced (Fig. 7B and 9B), and based on electron microscopy studies this reduction is unlikely to be due to myofibrillar disarray (Fig. 3B). This conclusion is supported by the studies on the maximal tension generation of single myofibrils (Fig. 7C): the magnitude of tension reduction in $Neb^{\Delta Exon55}$ myofibrils was similar to that in $Neb^{\Delta Exon55}$ fibres (62% and 64%, respectively). Thus, the weakness of muscle fibres in $Neb^{\Delta Exon55}$ mice can be attributed to changes in myofibrillar function, rather than by myofibrillar disarray or by a reduced myofibrillar fractional area. Note that the maximal tension generated by myofibrils was higher than that by muscle fibres, both in wild-type and $Neb^{\Delta Exon55}$ mice, and that this is caused by the tension in fibres being normalized to a cross-sectional area that comprises myofibrils plus non-contractile material such as mitochondria, glycogen granules and sarcoplasmic reticulum. The 64% reduction in tension generation by fibres from $Neb^{\Delta Exon55}$ muscle, combined with the reduction in fibre diameter of 23%, results in a total force loss of $>80\%$ in $Neb^{\Delta Exon55}$ fibres when compared with wild-type fibres. This severe muscle fibre weakness in $Neb^{\Delta Exon55}$ mice explains why the mice die within several days of birth, as this will severely hamper both feeding (the stomachs of $Neb^{\Delta Exon55}$ mice are typically devoid of milk) and breathing. That many patients homozygous for deletion of *NEB* exon 55 have been shown to survive past the neonatal phase (Anderson *et al*., 2004; Lehtokari *et al*., 2006, 2009; Ottenheijm *et al*., 2009*b*, 2010) is likely to be partly due to the extensive medical care that includes gastro-nasal feeding and mechanical ventilation. It should be noted that some patients with deletion of *NEB* exon 55, those with the typical form of nemaline myopathy, remain ambulant into adolescence or beyond. Future studies should address whether these patients have higher nebulin protein levels and a better preserved myofibrillar function.

The reduction in tension that we found in the mouse might be due to any of the myofibrillar functions that nebulin has been proposed to play: (i) specifying thin filament length; (ii) regulating the interaction between myosin-based crossbridges and the thin filament; and (iii) tuning the response of the thin filament to calcium (Bang *et al*., 2009; Chandra *et al*., 2009; Ottenheijm and Granzier, 2010;). Our work on the $Neb^{\Delta Exon55}$ mice indicates that all three mechanisms are disturbed upon deletion of *Neb* exon 55, and contribute to the development of muscle weakness.

In skeletal muscle, thin filament lengths are fine-tuned at ~1.1–1.3 μm (depending on species and muscle type) (Littlefield and Fowler, 2008) to overlap with thick filaments and to meet the muscle's contractile requirements (Burkholder *et al*., 1994; Littlefield and Fowler, 2008). The extent of overlap between thick and thin filaments determines the sarcomere's force generating capacity: short thin filaments reduce overlap and impair force generation. Thus, thin filament length is a key aspect of muscle function, and recent work indicates that nebulin is involved in specifying this length (Bang *et al*., 2006; Witt *et al*., 2006). Our immunofluorescence confocal microscopy studies revealed that thin filament length is significantly reduced from 1.0 μm in wild-type muscle to 0.85 μm in $Neb^{\Delta Exon55}$ muscle. These structural studies were corroborated by mechanical studies, which revealed a leftward shift (at sarcomere lengths of 2.4 μm and longer) of the force–sarcomere length relation in $Neb^{\Delta Exon55}$ muscle fibres. Thus, deletion of *Neb* exon 55 results in shorter thin filament lengths, contributing to muscle weakness at longer sarcomere lengths.

Weakness of $Neb^{\Delta Exon55}$ fibres was also apparent at sarcomere lengths shorter than 2.4 μm (Fig. 7B), suggesting that the reduction of thin filament length is not the only mechanism for weakness in $Neb^{\Delta Exon55}$ mice. Our findings show that crossbridge cycling kinetics in $Neb^{\Delta Exon55}$ fibres are altered, and that this contributes to muscle weakness. $Neb^{\Delta Exon55}$ muscle fibres had significantly higher tension cost compared to wild-type fibres (Fig. 8B), which indicates that the crossbridge detachment rate is higher (Stienen *et al*., 1996). In combination with the observation that k_{tr} was slower in $Neb^{\Delta Exon55}$ fibres (Fig. 8A), these findings lead to the conclusion that the rate of crossbridge attachment is slower in $Neb^{\Delta Exon55}$ fibres. Consequently, the fraction of force generating crossbridges is significantly reduced in $Neb^{\Delta Exon55}$ muscle. Importantly, these findings on $Neb^{\Delta Exon55}$ fibres were strongly supported by results from studies on single myobrils (Fig. 8C and D). The advantages of studies on myofibrils include that, due to their small size, they instantly equilibrate with the bathing solution making it possible to study force relaxation kinetics. Furthermore, as myofibrillar damage typically results in breakage of the myofibrils during activation, the data obtained from myofibrils reflect direct effects of the mutated protein on crossbridge cycling kinetics without potential confounding effects of myofibrillar damage. Importantly, the magnitude of the k_{tr} changes in myofibrils were similar to that in fibres and the changes in slow k_{rel} of myofibrils are similar to that of the tension cost measured in fibres. Thus, measurement at two distinct levels of organization (myofibrils and fibres) and using distinct techniques (tension cost measurements and force relaxation kinetics) support the hypothesis that alterations in crossbridge cycling kinetics greatly contribute to the observed weakness of $Neb^{\Delta Exon55}$ muscle.

The studies discussed above were carried out at a maximal activating calcium level. However, *in vivo*, skeletal muscle typically is submaximally activated. Thus, submaximal parameters of muscle function provide relevant physiological information. To test whether submaximal force generation was affected in $Neb^{\Delta Exon55}$ fibres, we exposed permeabilized fibres to various calcium concentrations and determined the ensuing force level. We found that the calcium sensitivity of force generation was significantly reduced in $Neb^{\Delta Exon55}$ fibres, suggesting that in addition to

maximal force generation, the capacity for submaximal force generation is greatly impaired in *Neb*$^{\Delta Exon55}$ mice.

In summary, muscle of *Neb*$^{\Delta Exon55}$ mice is nebulin-deficient and produces weakness by shortening thin filament lengths, reducing the fraction of crossbridges in the force generating state, and reducing the force response to submaximal calcium concentrations.

Troponin activation: a therapeutic mechanisms to improve muscle strength?

To date, no therapy exists that enhances force generation in patients with nemaline myopathy with nebulin mutations. Strategies to restore thin filament length or crossbridge cycling kinetics currently do not exist for skeletal muscle and, in part due to the extremely large size of the nebulin gene and protein, effective genetic strategies to combat these effects through gene therapy are likely far off in the future. However, the lower calcium sensitivity of force generation in patients with nemaline myopathy with nebulin mutations (Ottenheijm *et al*., 2010) might offer a more immediate therapeutic target, since a fast skeletal muscle troponin activator has been developed that amplifies the response of the thin filament to calcium in fast skeletal muscle fibres (Russell *et al*., 2012). The fast skeletal muscle troponin activator 'tirasemtiv' (formerly CK-2017357) was shown to greatly increase the calcium-sensitivity of force generation in healthy rat skeletal muscle fibres (Russell *et al*., 2012), and is currently in phase IIa clinical studies for generalized myasthenia gravis, and IIb clinical trials for amyotrophic lateral sclerosis (Shefner *et al*., 2012).

Here we took advantage of the novel *Neb*$^{\Delta Exon55}$ model to test the ability of the fast skeletal troponin activator CK-2066260 to improve muscle fibre strength in *Neb*$^{\Delta Exon55}$ fibres. CK-2066260 is a close structural analogue of tirasemtiv and the pharmacology of the two compounds is the same *in vitro* and *in vivo*. Our findings indicate that CK-2066260 greatly increases force generation in *Neb*$^{\Delta Exon55}$ fibres to levels that even exceed those observed in untreated muscle cells from wild-type mice (Fig. 9B). Thus, fast skeletal troponin activation might offer a therapeutic strategy for the restoration of muscle strength in patients with nemaline myopathy with deletion of nebulin exon 55, and possibly in patients with other nebulin mutations. Future studies should address whether the *in vivo* administration of troponin activators to nebulin knockout mouse models, such as the *Neb*$^{\Delta Exon55}$ mice, improves their survival.

In conclusion, we have generated a mouse model in which *Neb* exon 55 is deleted to model a founder mutation seen frequently in patients with nemaline myopathy. This is the first nebulin-based model for nemaline myopathy. Our data indicate that the phenotype of *Neb*$^{\Delta Exon55}$ mice recapitulates important features that we observed previously in patients harbouring this particular mutation. This severe muscle weakness, which characterizes the phenotype of both the mouse model and patients, can be restored by a novel compound that augments the response of the thin filament to calcium.

Acknowledgements

We gratefully acknowledge the Genetic Engineering of Mouse models (GEMM) core and its Director Dr. Tom Doetschman for making the *Neb*$^{\Delta Exon55}$ mouse model. Immunofluorescence microscopy for muscle fibre size was performed using the Children's Research Institute's Imaging Core Facility at MCW.

Funding

This work was supported by generous support by 'A Foundation Building Strength for Nemaline Myopathy' a VIDI grant (016.126.319) from the Netherlands Organization for Scientific Research to C.O., by the EU-FP7 and ERARE (SarcoSi and NEMMYOP) to S.L. and C.O., by PRIN 2010-2011 of the Ministero Università e Ricerca (MIUR), and by NIH R01 AR053897 to H.G., K08 AR059750, L40 AR057721 to M.W.L., R01 AR044345 to A.H.B., and grant MDA201302 from the Muscular Dystrophy Association (USA). Electron microscopy was performed at the Microbiology and Molecular Genetic EM Facility at MCW, which is supported by grants from the NIH (1S10RR022412-01) and 'Advancing a Healthier Wisconsin Program' from the MCW.

References

Anderson SL, Ekstein J, Donnelly MC, Keefe EM, Toto NR, LeVoci LA, et al. Nemaline myopathy in the Ashkenazi Jewish population is caused by a deletion in the nebulin gene. Hum Genet 2004; 115: 185–90.

Bang ML, Caremani M, Brunello E, Littlefield R, Lieber RL, Chen J, et al. Nebulin plays a direct role in promoting strong actin-myosin interactions. FASEB J 2009; 23: 4117–25.

Bang ML, Li X, Littlefield R, Bremner S, Thor A, Knowlton KU, et al. Nebulin-deficient mice exhibit shorter thin filament lengths and reduced contractile function in skeletal muscle. J Cell Biol 2006; 173: 905–16.

Brenner B, Eisenberg E. Rate of force generation in muscle: correlation with actomyosin ATPase activity in solution. Proc Natl Acad Sci USA 1986; 83: 3542–6.

Buck D, Hudson BD, Ottenheijm CA, Labeit S, Granzier H. Differential splicing of the large sarcomeric protein nebulin during skeletal muscle development. J Struct Biol 2010; 170: 325–33.

Burkholder TJ, Fingado B, Baron S, Lieber RL. Relationship between muscle fiber types and sizes and muscle architectural properties in the mouse hindlimb. J Morphol 1994; 221: 177–90.

Castillo A, Nowak R, Littlefield KP, Fowler VM, Littlefield RS. A nebulin ruler does not dictate thin filament lengths. Biophys J 2009; 96: 1856–65.

Chandra M, Mamidi R, Ford S, Hidalgo C, Witt C, Ottenheijm C, et al. Nebulin alters cross-bridge cycling kinetics and increases thin filament activation: a novel mechanism for increasing tension and reducing tension cost. J Biol Chem 2009; 284: 30889–96.

Engel AG, Gomez MR. Nemaline (Z disk) myopathy: observations on the origin, structure, and solubility properties of the nemaline structures. J Neuropathol Exp Neurol 1967; 26: 601–19.

Gokhin DS, Bang ML, Zhang J, Chen J, Lieber RL. Reduced thin filament length in nebulin-knockout skeletal muscle alters isometric contractile properties. Am J Physiol Cell Physiol 2009; 296: C1123–32.

Granzier HL, Akster HA, Ter Keurs HE. Effect of thin filament length on the force-sarcomere length relation of skeletal muscle. Am J Physiol 1991; 260: C1060–70.

Granzier HL, Wang K. Interplay between passive tension and strong and weak binding cross-bridges in insect indirect flight muscle. A functional dissection by gelsolin-mediated thin filament removal. J Gen Physiol 1993; 101: 235–70.

Greer KA, McReynolds MR, Brooks HL, Hoying JB. CARMA: a platform for analyzing microarray datasets that incorporate replicate measures. BMC Bioinformatics 2006; 7: 149.

Jin JP, Wang K. Cloning, expression, and protein interaction of human nebulin fragments composed of varying numbers of sequence modules. J Biol Chem 1991; 266: 21215–23.

Jungbluth H, Sewry CA, Counsell S, Allsop J, Chattopadhyay A, Mercuri E, et al. Magnetic resonance imaging of muscle in nemaline myopathy. Neuromuscul Disord 2004; 14: 779–84.

Kazmierski ST, Antin PB, Witt CC, Huebner N, McElhinny AS, Labeit S, et al. The complete mouse nebulin gene sequence and the identification of cardiac nebulin. J Mol Biol 2003; 328: 835–46.

Labeit S, Gibson T, Lakey A, Leonard K, Zeviani M, Knight P, et al. Evidence that nebulin is a protein-ruler in muscle thin filaments. FEBS Lett 1991; 282: 313–6.

Labeit S, Kolmerer B. The complete primary structure of human nebulin and its correlation to muscle structure. J Mol Biol 1995; 248: 308–15.

Lawlor MW, Ottenheijm CA, Lehtokari VL, Cho K, Pelin K, Wallgren-Pettersson C, et al. Novel mutations in NEB cause abnormal nebulin expression and markedly impaired muscle force generation in severe nemaline myopathy. Skelet Muscle 2011; 1: 23.

Lehtokari VL, Greenleaf RS, DeChene ET, Kellinsalmi M, Pelin K, Laing NG, et al. The exon 55 deletion in the nebulin gene—one single founder mutation with world-wide occurrence. Neuromuscul Disord 2009; 19: 179–81.

Lehtokari VL, Pelin K, Sandbacka M, Ranta S, Donner K, Muntoni F, et al. Identification of 45 novel mutations in the nebulin gene associated with autosomal recessive nemaline myopathy. Hum Mutat 2006; 27: 946–56.

Littlefield RS, Fowler VM. Thin filament length regulation in striated muscle sarcomeres: pointed-end dynamics go beyond a nebulin ruler. Semin Cell Dev Biol 2008; 19: 511–9.

McElhinny AS, Kazmierski ST, Labeit S, Gregorio CC. Nebulin: the nebulous, multifunctional giant of striated muscle. Trends Cardiovasc Med 2003; 13: 195–201.

Morris EP, Nneji G, Squire JM. The three-dimensional structure of the nemaline rod Z-band. J Cell Biol 1990; 111: 2961–78.

North KN, Laing NG, Wallgren-Pettersson C. Nemaline myopathy: current concepts. The ENMC International Consortium and Nemaline Myopathy. J Med Genet 1997; 34: 705–13.

Ochala J, Lehtokari VL, Iwamoto H, Li M, Feng HZ, Jin JP, et al. Disrupted myosin cross-bridge cycling kinetics triggers muscle weakness in nebulin-related myopathy. FASEB J 2011; 25: 1903–13.

Ogut O, Hossain MM, Jin JP. Interactions between nebulin-like motifs and thin filament regulatory proteins. J Biol Chem 2003; 278: 3089–97.

Ottenheijm CA, Granzier H. Lifting the nebula: novel insights into skeletal muscle contractility. Physiology (Bethesda) 2010; 25: 304–10.

Ottenheijm CA, Hidalgo C, Rost K, Gotthardt M, Granzier H. Altered contractility of skeletal muscle in mice deficient in titin's M-band region. J Mol Biol 2009a; 393: 10–26.

Ottenheijm CA, Hooijman P, DeChene ET, Stienen GJ, Beggs AH, Granzier H. Altered myofilament function depresses force generation in patients with nebulin-based nemaline myopathy (NEM2). J Struct Biol 2010; 170: 334–43.

Ottenheijm CA, Lawlor MW, Stienen GJ, Granzier H, Beggs AH. Changes in cross-bridge cycling underlie muscle weakness in patients with tropomyosin 3-based myopathy. Hum Mol Genet 2011; 20: 2015–25.

Ottenheijm CA, Witt CC, Stienen GJ, Labeit S, Beggs AH, Granzier H. Thin filament length dysregulation contributes to muscle weakness in nemaline myopathy patients with nebulin deficiency. Hum Mol Genet 2009b; 18: 2359–69.

Pappas CT, Krieg PA, Gregorio CC. Nebulin regulates actin filament lengths by a stabilization mechanism. J Cell Biol 2010; 189: 859–70.

Pelin K, Hilpela P, Donner K, Sewry C, Akkari PA, Wilton SD, et al. Mutations in the nebulin gene associated with autosomal recessive nemaline myopathy. Proc Natl Acad Sci USA 1999; 96: 2305–10.

Poggesi C, Tesi C, Stehle R. Sarcomeric determinants of striated muscle relaxation kinetics. Pflugers Arch 2005; 449: 505–17.

Russell AJ, Hartman JJ, Hinken AC, Muci AR, Kawas R, Driscoll L, et al. Activation of fast skeletal muscle troponin as a potential therapeutic approach for treating neuromuscular diseases. Nat Med 2012; 18: 452–5.

Ryan MM, Ilkovski B, Strickland CD, Schnell C, Sanoudou D, Midgett C, et al. Clinical course correlates poorly with muscle pathology in nemaline myopathy. Neurology 2003; 60: 665–73.

Sambuughin N, Swietnicki W, Techtmann S, Matrosova V, Wallace T, Goldfarb L, et al. KBTBD13 interacts with Cullin 3 to form a functional ubiquitin ligase. Biochem Biophys Res Commun 2012; 421: 743–9.

Sambuughin N, Yau KS, Olive M, Duff RM, Bayarsaikhan M, Lu S, et al. Dominant mutations in KBTBD13, a member of the BTB/Kelch family, cause nemaline myopathy with cores. Am J Hum Genet 2010; 87: 842–7.

Sanoudou D, Beggs AH. Clinical and genetic heterogeneity in nemaline myopathy—a disease of skeletal muscle thin filaments. Trends Mol Med 2001; 7: 362–8.

Shefner J, Cedarbaum JM, Cudkowicz ME, Maragakis N, Lee J, Jones D, et al. Safety, tolerability and pharmacodynamics of a skeletal muscle activator in amyotrophic lateral sclerosis. Amyotroph Lateral Scler 2012; 13: 430–8.

Shimomura C, Nonaka I. Nemaline myopathy: comparative muscle histochemistry in the severe neonatal, moderate congenital, and adult-onset forms. Pediatr Neurol 1989; 5: 25–31.

Stienen GJ, Kiers JL, Bottinelli R, Reggiani C. Myofibrillar ATPase activity in skinned human skeletal muscle fibres: fibre type and temperature dependence. J Physiol 1996; 493 (Pt 2): 299–307.

Tesi C, Piroddi N, Colomo F, Poggesi C. Relaxation kinetics following sudden Ca(2+) reduction in single myofibrils from skeletal muscle. Biophys J 2002; 83: 2142–51.

Warren CM, Krzesinski PR, Greaser ML. Vertical agarose gel electrophoresis and electroblotting of high-molecular-weight proteins. Electrophoresis 2003; 24: 1695–702.

Witt CC, Burkart C, Labeit D, McNabb M, Wu Y, Granzier H, et al. Nebulin regulates thin filament length, contractility, and Z-disk structure *in vivo*. EMBO J 2006; 25: 3843–55.

Yamaguchi M, Robson RM, Stromer MH, Dahl DS, Oda T. Actin filaments form the backbone of nemaline myopathy rods. Nature 1978; 271: 265–7.

Yamaguchi M, Robson RM, Stromer MH, Dahl DS, Oda T. Nemaline myopathy rod bodies. Structure and composition. J Neurol Sci 1982; 56: 35–56.